ECS Journal of Solid State
Science and Technology

OPEN ACCESS

Sidewall Electrical Damage in β-Ga_2O_3 Rectifiers Exposed to Ga^+ Focused Ion Beams

To cite this article: Xinyi Xia *et al* 2023 *ECS J. Solid State Sci. Technol.* **12** 055003

ECS Journal of Solid State Science and Technology, 2023 **12** 055003

Sidewall Electrical Damage in β-Ga_2O_3 Rectifiers Exposed to Ga^+ Focused Ion Beams

Xinyi Xia,[1,z] Nahid Sultan Al-Mamun,[2] Fan Ren,[1] Aman Haque,[2] and S.J. Pearton[3]

[1]*Department of Chemical Engineering, University of Florida, Gainesville FL 32611, United States of America*
[2]*Department of Mechanical Engineering, Penn State University, University Park, PA 16802, United States of America*
[3]*Department of Material Science and Engineering, University of Florida, Gainesville FL 32611, United States of America*

The energy and beam current dependence of Ga^+ focused ion beam milling damage on the sidewall of vertical rectifiers fabricated on n-type Ga_2O_3 was investigated with 5–30 kV ions and beam currents from 1.3–20 nA. The sidewall damage was introduced by etching a mesa along one edge of existing Ga_2O_3 rectifiers. We employed on-state resistance, forward and reverse leakage current, Schottky barrier height, and diode ideality factor from the vertical rectifiers as potential measures of the extent of the ion-induced sidewall damage. Rectifiers of different diameters were exposed to the ion beams and the "zero-area" parameters extracted by extrapolating to zero area and normalizing for milling depth. Forward currents degraded with exposure to any of our beam conductions, while reverse current was unaffected. On-state resistance was found to be most sensitive of the device parameters to Ga^+ beam energy and current. Beam current was the most important parameter in creating sidewall damage. Use of subsequent lower beam energies and currents after an initial 30 kV mill sequence was able to reduce residual damage effects but not to the point of initial lower beam current exposures.

 [DOI: 10.1149/2162-8777/acce6a]

Manuscript received March 15, 2023. Published May 4, 2023.

Focused ion milling of Ga_2O_3 is used for device mesa patterning, localized implantation, sample preparation for transmission electron microscopy and potentially for future microcircuit editing.[1–5] Ion beams play a crucial role in Atomic Layer Etch (ALE) sequences, offering precise etch rates, surface smoothing, and reduced surface damage compared to conventional RIE and ICP RIE. Typically, exposure to the focused beam induces a near-surface damage region up to 30 nm thick.[1] Methods to reduce FIB damage to semiconductors include the use of lower energies or subsequent wet or dry etching and cleaning.[6,7] This is particularly important in the main application of Ga_2O_3, which is power electronic devices. Some of these applications for Ga_2O_3 arise from the need for bidirectional switching of power, include electric vehicles (EVs) and their associated charging infrastructure with interfaces to the grid and home, as well as solid-state circuit breakers and distributed and grid-tie renewable power systems.

A wide variety of Ga_2O_3 devices with promising performance have been reported.[8–16] In both vertical rectifiers and lateral transistor structures, the presence of residual ion beam damage after mesa isolation or milling to create fins or trenches will be detrimental to device performance,[8–17] through inducing additional leakage current or creating additional parasitics. While ion-enhanced diffusion[18–21] of point defects created on horizontal semiconductor surfaces is known to produce damage depths well beyond those expected from ion range simulations,[22,23] there is limited understanding of the damage produced on a mesa sidewall in β-Ga_2O_3. There has been recent work on controlling sidewall angle during plasma etching, but no discussion of damage.[24]

In this paper we report a study to quantify the FIB sidewall damage in mesas on vertical Ga_2O_3 rectifiers. We measure changes in forward and reverse current, on-state resistance, barrier height, and ideality factor of Schottky contacts after creating a sidewall on the rectifiers by ion beam exposure of the Ga_2O_3 surface under different FIB beam energies, current and beam sequence. Different device diameters were examined, and the zero-area values of the electrical parameters established by extrapolation. Beam current was found to be the most critical parameter in creating damage. The use of subsequent lower beam energies and currents after an initial 30 kV mill sequence reduced residual damage effects but not to the extent of initial lower beam current exposures.

Experimental

The energy range of the Ga^+ ions was 5 kV to 30 kV, with beam currents from 1.3–20 nA. The lateral straggle of ions in this energy range is <10 nm,[22,23] though, as noted previously, ion-enhanced diffusion of defects is expected.[1,18–21] We used vertical rectifier structures as our platform for investigating the FIB-induced sidewall damage. These consisted of 10 μm thick, lightly Si doped epitaxial layers grown by halide vapor phase epitaxy (HVPE) with carrier concentration 2×10^{16} cm^{-3}, grown on a (001) surface orientation Sn-doped β-Ga_2O_3 single crystal (Novel Crystal Technology, Japan). A full area Ti/Au backside Ohmic contact was formed by e-beam evaporation and was annealed at 550 °C for 1 min under N_2 ambient.

The samples were processed as shown schematically in Figure 1. Details of the device fabrication have been given elsewhere.[25] The edge of completed rectifiers were exposed to focused Ga^+ ions at normal incidence to create a sidewall mesa. The milling depth was kept constant at $\sim$1 μm, while the square or rectangular milled areas were 10×10, 10×30 or 10×50 μm^2. The approximate milling rates for the Ga_2O_3 were 15, 6 and 2.75 μm^3 s^{-1} for 30, 10 and 5 kV, respectively. Figure 2 shows the patterned area at the edge of the rectifiers before and after milling under different beam energies and currents. The highest energies led to some degradation of metal morphology on the Schottky contact. Notably, the openings for reference diodes were not created by FIB; instead, they were produced through patterning.

The current density-voltage (J-V) characteristics before and after milling of the mesas were recorded with Agilent 4156C. We have previously established that thermionic emission is the main current conduction mechanism in the rectifiers prior to mesa formation.[1] The on-state resistance R_{on} is given by:

$$R_{on} = \frac{W_N}{e\mu_n N_d}$$

where the drift layer depletion thickness is W_N, the doping in the drift region is Nd, e is the electronic charge and μ_n is the electron mobility. The R_{on} was obtained from the slope of the forward J-V characteristics. The barrier height Φ_b and ideality factor were extracted from the current density J relation[26]

[z]E-mail: spear@mse.ufl.edu

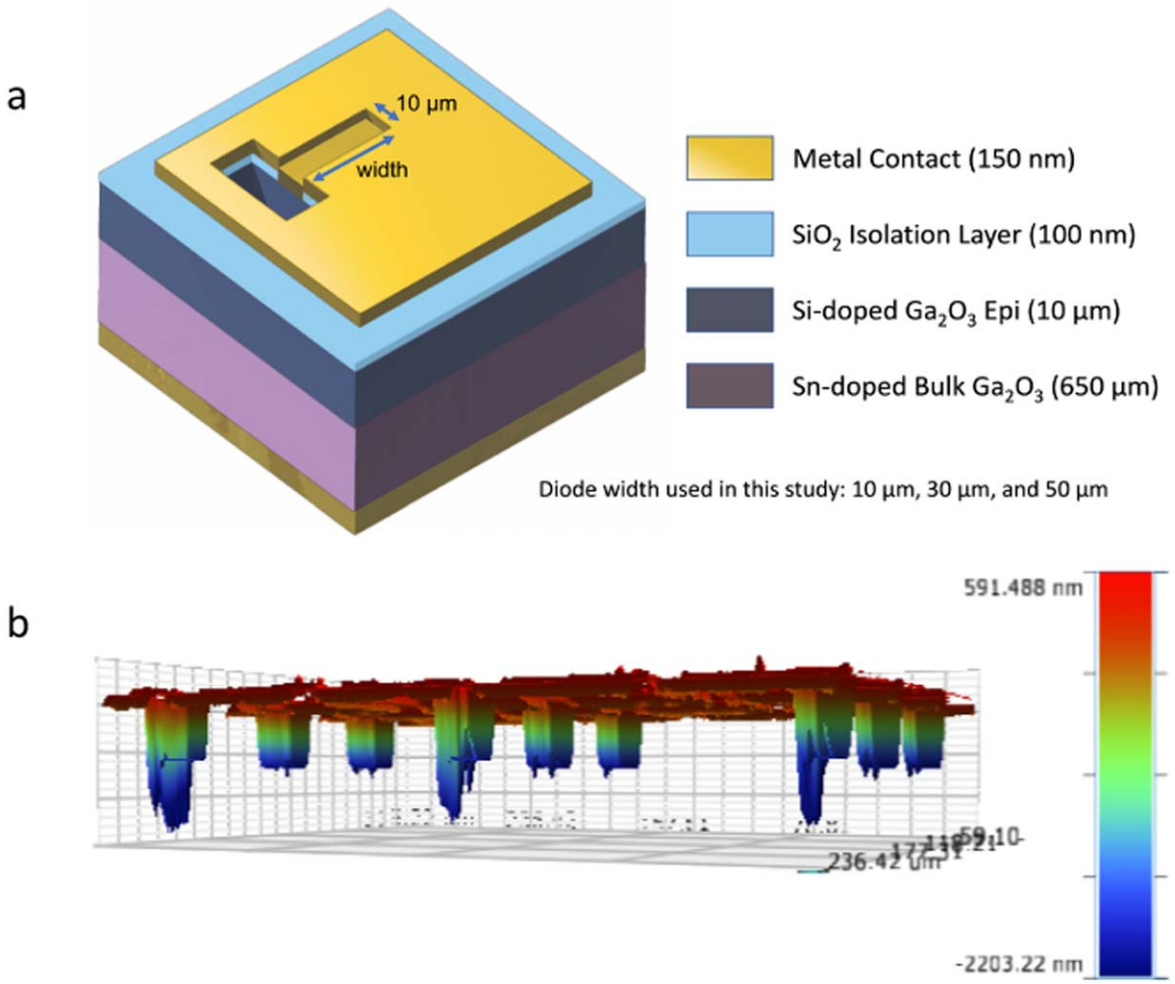

Figure 1. (a) Schematic of Schottky rectifier and subsequent creation of milled region along one edge to create sidewall damage. (b) Optical profilometer 3D topography scan of milled areas.

$$J = A^{*}T^{2}\exp\left(-e(\Phi_B - \Delta\Phi)/k_B T\right)\exp\left[(eV/nk_BT) - 1\right]$$

where A* is the Richardson constant, T is absolute temperature, e the electronic charge, $\Delta\Phi$ is the image force barrier lowering and k_B is Boltzmann's constant. We used the changes in on-resistance, barrier height and ideality factor because of ion beam exposure as a quantitative measure of the magnitude of the ion-induced sidewall damage for the beam energy and current combinations.

For each parameter, we conducted normalization with respect to both area and milling depth. Using R_{on} as an example, we initially normalized the reference sample's R_{on} measurement based on the actual diode area to account for variations in the measurement area size. Subsequently, to address differences attributable to FIB damage, we subtracted the reference sample's R_{on} measurement from the R_{on} measurement of each individual diode. In order to account for potential variations in measurement depth, we normalized the R_{on} measurement to a depth of 1 μm. To extrapolate the normalized R_{on}, we created a linear trend line using normalized R_{on} values from two groups with different diode sizes. The *x*-axis intercept of this trend line represents the extrapolated normalized R_{on} value. In essence, we plotted the normalized R_{on} values from each group on a graph, drew a trend line through the data points, and extended this line beyond the range of the plotted data points to estimate the normalized R_{on} value for a diode size outside the measured range. The *x*-axis intercept represents this estimated value, which is the extrapolated normalized R_{on}. A similar approach was applied for ideality factor and barrier height. First, we normalized measurements according to the actual diode area to account for size variations. Next, we subtracted the reference sample's measurement from each diode's measurement to address FIB damage differences. After normalizing measurements to a 1 μm depth to account for potential depth variations, we extrapolated the normalized values to eliminate diode size effects.

Results and Discussion

Figure 3 displays the forward J-V characteristics and associated on-state resistances from rectifiers with sidewall mesa milled under various energy and current conditions. In comparison to the reference device, the sidewall damage caused by Ga^{+} ion beam milling leads to greater degradation in the forward current density as energy and, in particular, exposure time to the beam increase, along with the increase in cut depth. For instance, the most significant current loss occurs in the sequence where we initially milled with 30 kV energy, then attempted to remove some of the resulting damaged region by employing lower current, followed by a similar energy at a comparable current. This outcome is also reflected in the higher on-resistances. The reduction in current is primarily due to acceptor trap formation, which decreases the carrier density in the damaged regions.[1]

The Φ_B, n and R_{on} values before and after ion beam exposure are shown in Table I. Note that the extracted barrier height includes the barrier image force lowering, $\Delta\Phi$. We use the extracted device parameters as an indicator of damage introduction or removal. The Richardson's constant was calculated to be in the range

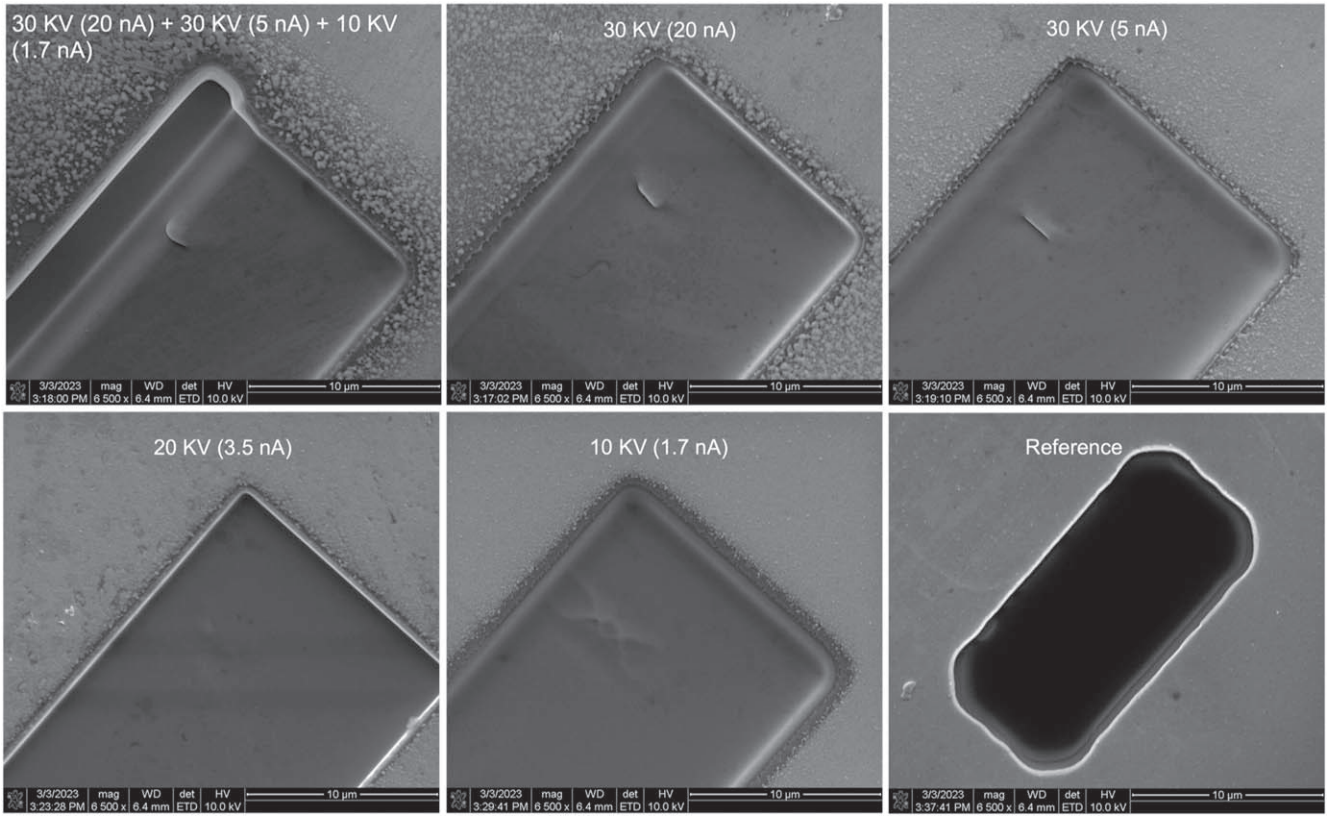

Figure 2. SEM micrographs of features prior to milling and after milling at different conditions.

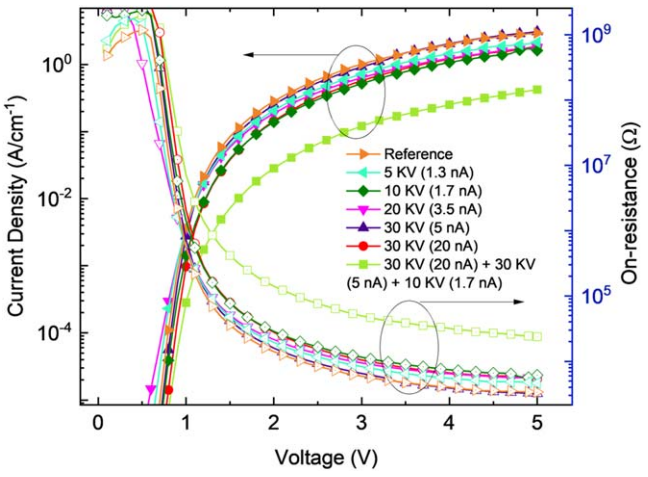

Figure 3. Forward current density-voltage characteristics (closed symbols) and extracted on-resistances (open symbols) from rectifiers before and after sidewall damage milling at different energies and beam currents.

28.8–41.8 A $cm^{-2}K^{-2}$ for the diodes still exhibiting ideality factors ~2, which again are consistent with literature values.[27–29] Even for a 5 kV exposure, the ideality factor increases beyond its original value, which is indicative of a strong contribution from other conduction mechanisms like defect-assisted tunneling and recombination.

In contrast to the reductions in forward currents, the reverse J-V characteristics, shown in Figure 4 display an increase in reverse current density for devices after FIB milling. This arises from the additional generation-recombination contribution from the damage-induced trap states. The main defects produced in Ga_2O_3 by energetic ions beams are Ga vacancies (V_{Ga}), which can be triple acceptors depending on the Fermi level position.[30,31] These V_{Ga} species are known to diffuse rapidly in Ga_2O_3, and this may be enhanced in the presence of the high level of electronic excitation during the ion beam exposure.[31] While the calculated threshold energies for displacement are 28 eV for Ga and 14 eV for O,[32] the recombination rate of the latter are much higher, leaving Ga defects as the main influence on the electrical properties of the β-Ga_2O_3.

Figure 5 presents the extrapolated normalized R_{on} values for different beam conditions and sequences. Additionally, we included plots of extrapolation without normalizing the FIB cut depth for

Table I. Typical device parameters for rectifiers with 10 × 30 μm mesa formed by ion milling at different beam conditions.

	R_{on} (mΩ.cm^2)	Size (μm^2)	Depth (μm)	Normalized R_{on}
30 KV (20 nA) + 30 KV (5 nA) + 10 KV (1.7 nA)	418.5	10 × 21	2.1	267.36
30 KV (20 nA)	71.9	10 × 20	1.1	64.95
30 KV (5 nA)	54.8	10 × 21	1.1	38.07
20 KV (3.5 nA)	55.4	10 × 20	0.83	56.26
10 KV (1.7 nA)	52.5	10 × 22	0.83	42.39
5 KV (1.3 nA)	49.3	10 × 24	0.59	42.75

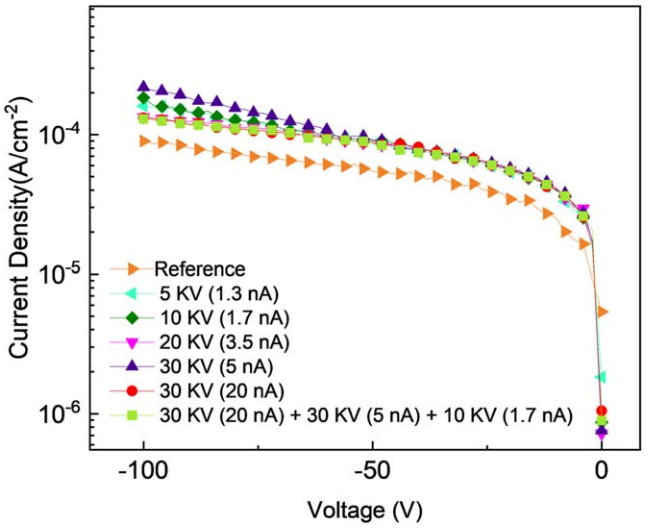

Figure 4. Reverse current density-voltage characteristics from rectifiers before and after sidewall damage milling at different energies and beam currents.

These findings suggest that beam current is the most critical parameter in creating sidewall damage. Employing subsequent lower beam energies and currents after an initial 30 kV mill sequence can reduce residual damage effects, although not to the extent of initial lower beam current exposures.

Conclusions

Sidewall damage in Ga_2O_3 rectifiers caused by Ga^+ ion beams was investigated as a function of ion energy (5–30 kV), current, and beam parameter sequence. The values for Ron, ideality factor, and Schottky barrier height were determined by normalizing the reference value to the size of each diode, subtracting the normalized reference value, and extrapolating to eliminate the effect of size. The electrical characteristics of Schottky diodes after the creation of sidewall damage were sensitive to beam current and energy. A sequence employing high beam current and energy for rapid milling removal rate, followed by the use of lower energy beams to remove damage created at higher energies, proved successful and will be useful in practical device processing sequences.

Acknowledgments

This work was funded by the Defense Threat Reduction Agency (DTRA) as part of the Interaction of Ionizing Radiation with Matter University Research Alliance (IIRM-URA) under contract number HDTRA1-20-2-0002. The work at UF was also supported by the NSF DMR 1856662. The work at PSU is also supported by the NSF ECCS 2015795. The content of the information does not necessarily reflect the position or the policy of the federal government, and no official endorsement should be inferred.

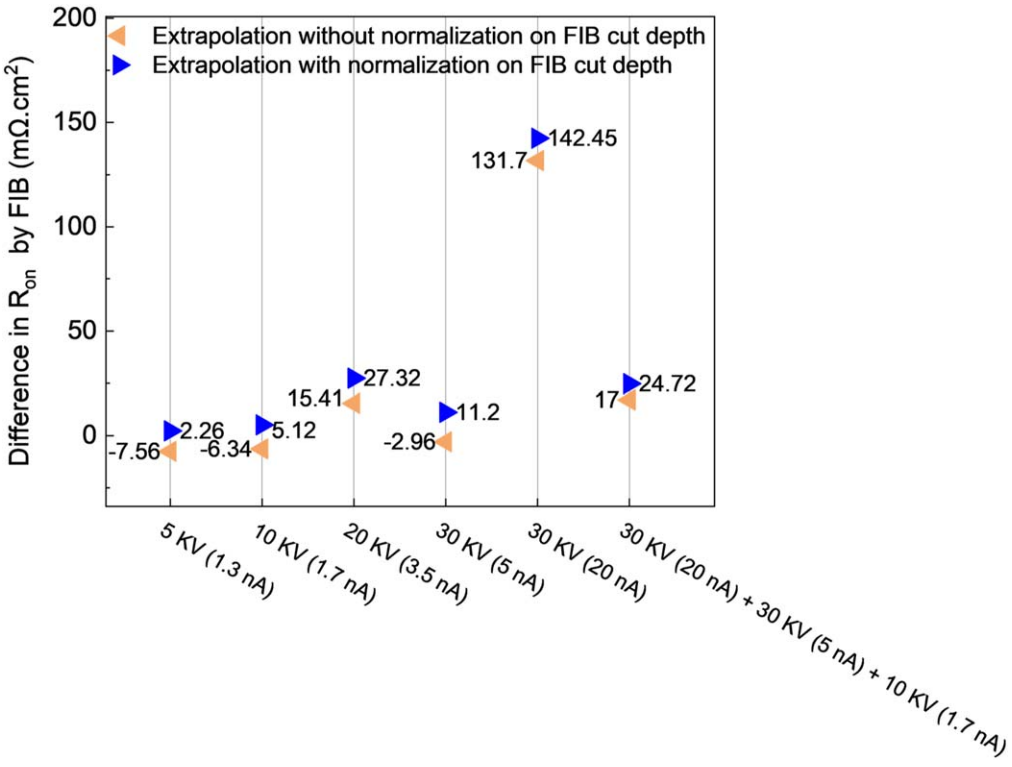

Figure 5. Extrapolated normalized R_{ON} for different FIB conditions.

comparison. The absolute values for the reference samples ranged from 31.2 to 69.1 mΩ.cm^2. It is important to note that for beam energies of 5–30 kV and low beam current (<5 nA), the changes in R_{on} are less than 30%. However, the combination of high energy and beam current results in significant increases in R_{on}, as evidenced by the 30 kV, 20 nA outcome. By employing progressively lower beam voltage and current to remove some of the damaged sidewall, the extent of degradation can be reduced.

Similar results are shown for ideality factor in Figure 6, where the difference between reference and damaged values is only significant for the 30 kV, 20 nA condition. Comparable trends are also evident in the Schottky barrier height data displayed in Figure 7.

ORCID

Xinyi Xia https://orcid.org/0000-0002-8644-8599
Aman Haque https://orcid.org/0000-0001-6535-5484
S.J. Pearton https://orcid.org/0000-0001-6498-1256

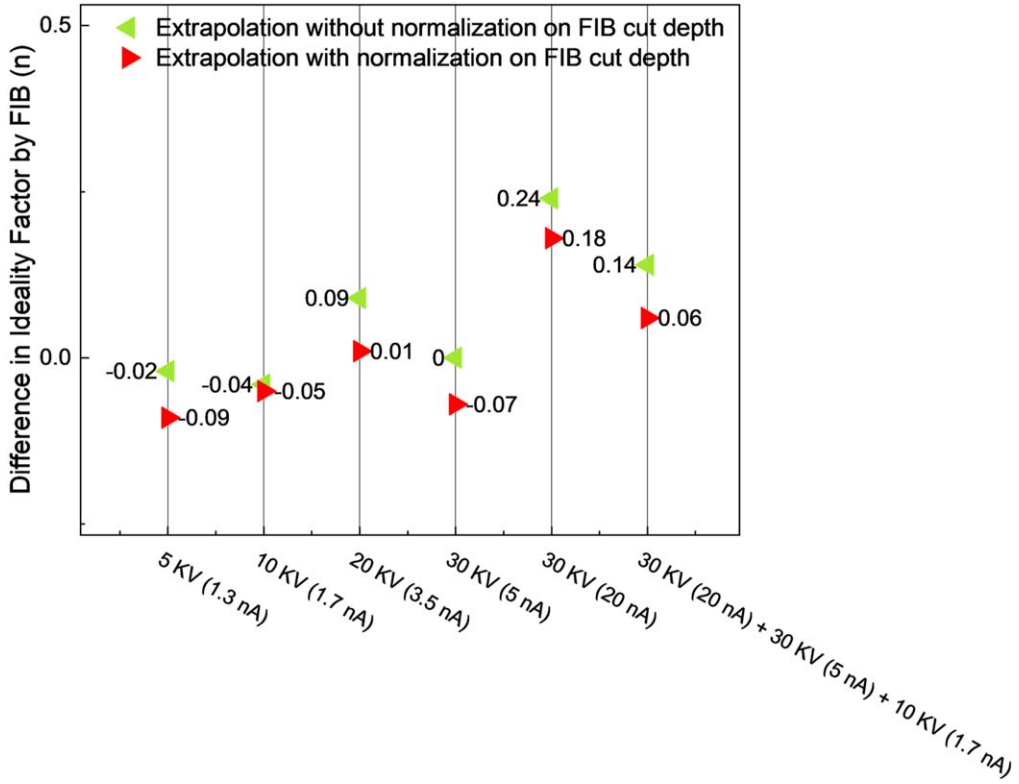

Figure 6. Extrapolated normalized ideality factor.

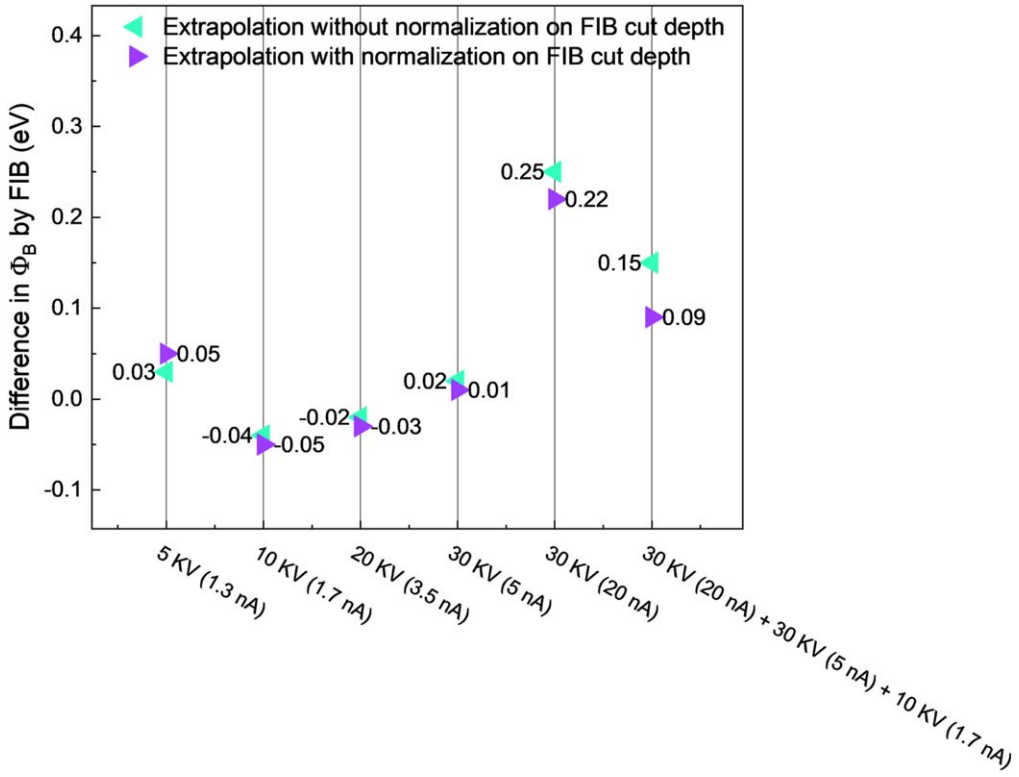

Figure 7. Extrapolated normalized Schottky barrier height.

References

1. X. Xia, N. Sultan Al-Mamun, D. Warywoba, F. Ren, A. Haque, and S. J. Pearton, *J. Vac Sc Technol. A*, **40**, 053403 (2022).
2. T. Ohba, W. Yang, S. Tan, K. J. Kanarik, and K. Nojiri, *Jpn. J. Appl. Phys.*, **56**, 06HB06 (2017).
3. D. Ohori, T. Sawada, K. Sugawara, M. Okada, K. Nakata, K. Inoue, D. Sato, H. Kurihara, and S. Samukawa, *J. Vac. Sci. Technol. A*, **38**, 032603 (2020).
4. Y. Lee, N. R. Johnson, and S. M. George, *Chem. Mater.*, **32**, 5937 (2020).

5. K. A. Hatch, D. C. Messina, and R. J. Nemanich, *J. Vac. Sci. Technol. A*, **40**, 042603 (2022).
6. N. I. Kato, *J. Electron Microscopy*, **53**, 451 (2004).
7. H.-K. Lee, H.-J. Yun, K.-H. Shim, H.-G. Park, T.-H. Jang, S.-N. Lee, and C.-J. Choi, *Appl. Surf. Sci.*, **506**, 144673 (2020).
8. M. H. Wong and M. Higashiwaki, *IEEE T Electron Dev*, **67**, 3925 (2020).
9. A. J. Green et al., *APL Mater.*, **10**, 029201 (2022).
10. S. J. Pearton, F. Ren, M. Tadjer, and J. Kim, *J. Appl. Phys.*, **124**, 220901 (2018).
11. E. Ahmadi and Y. Oshima, *J. Appl. Phys.*, **126**, 160901 (2019).
12. Y. Wang et al., *IEEE Trans Electron Dev*, **69**, 1945 (2022).
13. W. Li, D. Saraswat, Y. Long, K. Nomoto, D. Jena, and H. G. Xing, *Appl. Phys. Lett.*, **116**, 192101 (2020).
14. M. Xiao et al., *IEEE Trans. Power Electron.*, **36**, 8505 (2021).
15. N. K. Kalarickal, Z. Xia, H.-L. Huang, W. Moore, Y. Liu, M. Brenner, J. Hwang, and S. Rajan, *IEEE Electron Dev. Lett*, **42**, 899 (2021).
16. M. Zhang, Z. Liu, L. Yang, J. Yao, J. Chen, J. Zhang, W. Wei, Y. Guo, and W. Tang, *Crystals*, **12**, 406 (2022).
17. D. Kalanov, A. Anders, and C. Bundesmann, *J. Vac. Sci. Technol. A*, **39**, 053409 (2021).
18. J. Bourgoin, D. Peak, and J. W. Corbett, *J. Appl. Phys.*, **44**, 3022 (1973).
19. E. G. Seebauer and M. C. Kratzer, *Mat. Sci Eng R*, **55**, 57 (2006).
20. D. Stievenard, *Mat Sci. Eng B*, **71**, 120 (2000).
21. J. Bourgoin and J. W. Corbett, *Phys. Lett. A*, **38A**, 135 (1993).
22. J. Ziegler, J. P. Biersack, and M. D. Ziegler, *SRIM-The Stopping and Ranges of Ions in Solids* (SRIM Co., Chester) (2008), (www.srim.org).
23. J. F. Ziegler, J. P. Biersack, and U. Littmark, "The stopping and range of ions in solids." *The Stopping and Range of Ions in Matter* 1, ed. J. F. Ziegler (Pergamon, New York) (1985).
24. C. Bian et al., *Jpn. J. Appl. Phys.*, **62**, 011004 (2023).
25. J. Yang, F. Ren, M. Tadjer, S. J. Pearton, and A. Kuramata, *ECS J. Solid State Sci. Technol.*, **7**, Q92 (2018).
26. L. A. M. Lyle, K. Jiang, E. V. Favela, K. Das, A. Popp, Z. Galazka, G. Wagner, and L. M. Porter, *J. Vac. Sci. Technol. A*, **39**, 033202 (2021).
27. H. Sheoran, V. Kumar, and R. Singh, "A Comprehensive Review on Recent Developments in Ohmic and Schottky Contacts on Ga_2O_3 for Device Applications." *ACS Applied Electronic Materials*, **4**, 2589–628 (2022).
28. S. Mukhopadhyay, L. A. M. Lyle, H. Pal, K. K. Das, L. M. Porter, and B. Sarkar, "Evidence of thermionic emission in forward biased β-Ga_2O_3 Schottky diodes at Boltzmann doping limit." *J Appl Phys*, **131**, 025702 (2022).
29. L. A. M. Lyle, K. Jiang, E. V. Favela, K. Das, A. Popp, Z. Galazka, G. Wagner, and L. M. Porter, "Effect of metal contacts on (100) β-Ga_2O_3Schottky barriers." *J. Vac. Sci. Technol.*, A**39**, 033202 (2021).
30. S. J. Pearton et al., *ECS J. Solid State SC.*, **10**, 055008 (2021).
31. Y. K. Frodason, J. B. Varley, K. M. Johansen, L. Vines, and C. G. Van de Walle, *Phys. Rev. B*, **107**, 024109 (2023).
32. B. R. Tuttle, N. J. Karom, A. O'Hara, R. D. Schrimpf, and S. T. Pantelides, *J. Appl. Phys.*, **133**, 015703 (2023).